

Elegant solutions to the 96 GeV diphoton excess in the seesaw extensions of the natural NMSSM

Junjie Cao, Xinglong Jia, Yuanfang Yue, Haijing Zhou, and Pengxuan Zhu

Department of Physics, Henan Normal University, Xinxiang 453007, China

E-mail: junjiec@itp.ac.cn, 645665975@qq.com, yuanfang405@gmail.com,
zhouhaijing@htu.edu.cn, zhupx99@icloud.com

ABSTRACT: The Next-to Minimal Supersymmetric Standard Model (NMSSM) with a Type-I seesaw mechanism extends the NMSSM by three generations of right-handed neutrino fields to generate neutrino mass. As a byproduct it renders the lightest sneutrino as a viable DM candidate. Due to the gauge singlet nature of the DM, its scattering with nucleon is suppressed in most cases to coincide spontaneously with the latest XENON-1T results. Consequently, broad parameter spaces in the Higgs sector, especially a light Higgsino mass, are resurrected as experimentally allowed, which makes the theory well suited to explain the long standing $b\bar{b}$ excess at LEP-II and the continuously observed $\gamma\gamma$ excess by CMS collaboration. We show by both analytic formulas and numerical results that the theory can naturally predict the central values of the excesses in its broad parameter space, and the solutions are consistent with the Higgs data of the discovered Higgs boson, B -physics and DM physics measurements, the electroweak precision data as well as the LHC search for sparticles. Part of the solutions may be tested by future DM experiments and the SUSY search at the LHC.

Contents

1	Introduction	1
2	Theoretical preliminaries	4
2.1	NMSSM with the Type-I seesaw mechanism	4
2.2	Formula for the $b\bar{b}$ and $\gamma\gamma$ signals	7
3	Solutions to the excesses	8
3.1	Strategy in scanning the parameter space	9
3.2	Numerical Results	10
4	Constraints from DM physics and sparticle search	14
5	Conclusions	18

1 Introduction

Electroweak symmetry breaking (EWSB) is one of the most important issue in particle physics. The discovery of a Standard Model (SM) like Higgs boson at the Large Hadron Collider (LHC) [1, 2] indicates the correctness of Higgs mechanism, while the quadratically divergent correction to the boson mass in the SM implies the need of a more complex theoretical structure to account for the EWSB in a natural way. Without considering extreme cases, the complete EWSB mechanism should manifest itself by potentially sizable deviations (less than roughly 20% at 95% confidence level according to current Higgs data at the LHC [3]) of the boson’s property from its SM prediction, and/or by exotic signals at colliders. Interestingly, so far it seems that the latter has emerged through a 2.3σ local excess for the channel $e^+e^- \rightarrow Z\phi_{b\bar{b}} \rightarrow Zb\bar{b}$ at LEP-II with the scalar mass $m_{\phi_{b\bar{b}}} \sim 98$ GeV [4, 5], and also through a roughly 3σ local excess for the channel $pp \rightarrow \phi_{\gamma\gamma} \rightarrow \gamma\gamma$ at the LHC with $m_{\phi_{\gamma\gamma}} \simeq 96$ GeV, which was reported recently by CMS collaboration after combining 7, 8 and 13 TeV data [6, 7]¹. The normalized signal strengths of the excesses are [6, 10]

$$\begin{aligned}\mu_{\text{LEP}} &= \frac{\sigma(e^+e^- \rightarrow Z\phi_{b\bar{b}} \rightarrow Zb\bar{b})}{\sigma^{\text{SM}}(e^+e^- \rightarrow ZH_{\text{SM}} \rightarrow Zb\bar{b})} = 0.117 \pm 0.057, \\ \mu_{\text{CMS}} &= \frac{\sigma(gg \rightarrow \phi_{\gamma\gamma} \rightarrow \gamma\gamma)}{\sigma^{\text{SM}}(gg \rightarrow H_{\text{SM}} \rightarrow \gamma\gamma)} = 0.6 \pm 0.2.\end{aligned}\tag{1.1}$$

¹Recently the ATLAS collaboration also published its analysis of about 80 fb^{-1} data on the diphoton signal [8], and it claims no significant excess over the SM expectation for the diphoton mass below 110 GeV. As illustrated in Fig. 1 in Ref. [9], this conclusion does not conflict with the CMS result since the ATLAS analysis deals with a significantly larger background around Z peak.

Since the mass resolution for the $b\bar{b}$ final state at LEP-II is rather coarse [9] and at same time $\phi_{b\bar{b}}$ and $\phi_{\gamma\gamma}$ are so close in mass, it is commonly conjectured that the two excesses have same physical origin. So far a variety of beyond SM theories were studied to reveal it, where the intermediate scalar ϕ is usually taken as a gauge singlet CP-even Higgs or a singlet-like particle. These theories include the radion model [11, 12], the singlet extensions of the SM by additional vector-like matter fields [13, 14], the fermiophobia Type-I Two Higgs Doublet Model (2HDM) [13, 15], the singlet extensions of the 2HDM [16, 17] and its supersymmetric version (namely the Next-to-Minimal Supersymmetric Standard Model (NMSSM)) [9, 10, 18–21], as well as the μ -from- ν Supersymmetric Standard Model ($\mu\nu$ SSM) [22, 23]. Among these models, the NMSSM [24] is of particular interest because, due to the introduction of one singlet Higgs field, it has more theoretical advantages than the popular Minimal Supersymmetric Standard Model (MSSM), such as generating dynamically the μ -term, which is responsible for Higgsino mass, and providing more feasible dark matter (DM) candidates so that the model’s phenomenology is enriched greatly [25–28]. Moreover, as far as the light CP-even Higgs scenario of the model (which is appropriate to explain the excesses) is concerned, the mass of the SM-like Higgs boson can be significantly lifted up by both an additional tree-level contribution and the singlet-doublet mixing effect [29–31], which makes large radiative corrections from stop loops unnecessary in predicting $m_h \simeq 125$ GeV, and the Higgsino mass is upper bounded by about 400 GeV, which is the right range to predict Z boson mass in a natural way [30, 32, 33].

A thorough analysis of the light Higgs scenario in the general NMSSM was recently performed in [21] by both compact analytic formula and numerical results. It was concluded that there are parameter spaces where the excesses can be well explained without conflicting with the 125 GeV Higgs data collected at the LHC. With regard to such a study, we remind that, for the NMSSM as one of the most intensively studied supersymmetric theory, its parameter space in Higgs sector has been tightly limited by DM physics and also by the LHC search for sparticles [34], which should be considered in a comprehensive study of the excesses. The tightness of the constraints comes from following facts:

- In the NMSSM, the lightest neutralino (usually with Bino or Singlino field as its dominant component) is customarily taken as a DM candidate. Some parameters for the neutralino sector of the theory, such as λ , κ , $\tan\beta$ and μ , are also inputs of the Higgs sector [24]. Notably, besides affecting the Higgs mass spectrum, these parameters usually play an important role in determining the DM property, such as its mass, field component as well as interactions with Higgs and SM gauge bosons [35]. So they are restricted by the measurements in DM physics.
- Given that squarks and sleptons are preferred heavy by the direct search for sparticles at the LHC and consequently they have little effect on DM physics when $m_{\text{DM}} \sim 100$ GeV, the Higgs bosons and SM gauge bosons often act as the mediators or final states of DM annihilation. Then the DM relic density precisely measured by WMAP and Planck experiments [36] requires fine-tuned configurations of the involved parameters [35, 37].

- So far XENON-1T experiment has reached unprecedented sensitivity in detecting DM-nucleon scattering, i.e. $\sigma^{\text{SI}} \sim 10^{-47} \text{ cm}^2$ for spin-independent (SI) cross section [38] and $\sigma^{\text{SD}} \sim 10^{-41} \text{ cm}^2$ for spin-dependent (SD) cross section [39]. Since t-channel exchange of Higgs bosons (Z boson) is the dominant contribution to the SI (SD) cross section at tree level, the experiment can exclude a large portion of the parameter space in the Higgs sector, especially in case of light Higgsinos and/or light Higgs bosons where strong cancellation between different Higgs contributions must be present to coincide with the experimental results [40, 41].
- With the smooth progress of the LHC in looking for electroweakinos by multi-lepton signals, the mass spectrum of neutralinos and charginos has been tightly limited within certain patterns for $\mu \lesssim 500 \text{ GeV}$ [34].

In fact, we once studied the excesses in the NMSSM with a \mathbb{Z}_3 discrete symmetry by considering the constraints from LUX and PandaX experiments on DM-nucleon scattering in 2016. We found that they can be explained at 1σ level only in a very narrow parameter space and at the cost of relaxing the relic density constraint [10]. Since the latest XENON-1T results have improved the previous sensitivity by a factor of about 5, we checked that the space becomes experimentally disfavored [34].

Given the great theoretical advantages of the NMSSM and unfortunately the strong experimental constraints on its most natural parameter space, we were motivated to augment the NMSSM with different seesaw mechanisms to generate neutrino mass and also to enable the lightest sneutrino $\tilde{\nu}$ as a viable DM candidate [42–44]. The general feature of such extensions is that the singlet Higgs field plays extra roles [42, 43]: apart from being responsible for heavy neutrino mass via the interaction $\hat{S}\hat{\nu}\hat{\nu}$ in superpotential (\hat{S} and $\hat{\nu}$ denote the superfield of the singlet Higgs and the heavy neutrino respectively), it contributes to the annihilation of $\tilde{\nu}$ and consequently makes the property of $\tilde{\nu}$ compatible with various measurements in a natural way. This can be understood from two popular cases. One is that the singlet Higgs can mediate the transition between the $\tilde{\nu}$ pair and the Higgsino pair so that $\tilde{\nu}$ and the Higgsinos are in thermal equilibrium in early universe before their freeze-out. If their mass splitting is less than about 10%, the number density of the Higgsinos can track that of $\tilde{\nu}$ during freeze-out, and as a result the Higgsinos played a dominant role in determining the density due to its relatively strong interaction with SM particles [45] (in literature such a phenomenon was called coannihilation [46]). In this case, the constraint on the Higgsino mass μ from the LHC search for electroweakinos is rather weak due to the compressed spectrum, and light Higgsinos with $\mu \sim 100 \text{ GeV}$ are still allowed. The other is that, due to its gauge singlet nature, $\tilde{\nu}$ and the singlet Higgs can compose a secluded DM sector where the measured relic abundance can be accounted for by the annihilation of $\tilde{\nu}$ into a pair of the singlet Higgs. In both the cases, $\tilde{\nu}$ couples very weakly with the SM particles so that its scattering with nucleon is always suppressed, which is consistent with current DM direct detection (DD) results. This is a great theoretical advantage in light of the tight experimental limit. At this stage, we emphasize that, when one fixes the mass spectrum of the Higgs bosons and neutralinos, it usually happens that the theory is kept compatible with various DM measurements solely by adjusting the parameters in the

Superfield	Spin 0	Spin $\frac{1}{2}$	Generations	$(U(1) \otimes SU(2) \otimes SU(3))$
\hat{q}	\tilde{q}	q	3	$(\frac{1}{6}, \mathbf{2}, \mathbf{3})$
\hat{l}	\tilde{l}	l	3	$(-\frac{1}{2}, \mathbf{2}, \mathbf{1})$
\hat{H}_d	H_d	\tilde{H}_d	1	$(-\frac{1}{2}, \mathbf{2}, \mathbf{1})$
\hat{H}_u	H_u	\tilde{H}_u	1	$(\frac{1}{2}, \mathbf{2}, \mathbf{1})$
\hat{d}	\tilde{d}_R^*	d_R^*	3	$(\frac{1}{3}, \mathbf{1}, \bar{\mathbf{3}})$
\hat{u}	\tilde{u}_R^*	u_R^*	3	$(-\frac{2}{3}, \mathbf{1}, \bar{\mathbf{3}})$
\hat{e}	\tilde{e}_R^*	e_R^*	3	$(1, \mathbf{1}, \mathbf{1})$
\hat{s}	S	\tilde{S}	1	$(0, \mathbf{1}, \mathbf{1})$
$\hat{\nu}$	$\tilde{\nu}_R^*$	ν_R^*	3	$(0, \mathbf{1}, \mathbf{1})$

Table 1. Field content of the NMSSM with Type-I seesaw mechanism.

sneutrino sector [42–44]. This reflects the fact that, although the DM sector and the Higgs sector of the theory are entangled together to survive various experimental constraints, which is the same as the NMSSM, their correlation becomes loose and the constraints from DM physics are weakened greatly. This will resurrect broad parameter spaces in the Higgs sector as experimentally allowed and thus make the theory suitable to explain the excesses. Studying the capability of the augmented theory to explain the excesses is the main aim of this work.

This paper is organized as follows. In section 2, we first take the NMSSM with a Type-I seesaw mechanism as an example to recapitulate the basics of the more general framework where the NMSSM is augmented by different seesaw mechanisms, including its field content and Lagrangian, then we turn to discuss the conditions to produce sizable $b\bar{b}$ and $\gamma\gamma$ signals. In Section 3, we perform a comprehensive scan over the vast parameter space of the Higgs sector to look for the regions where the excesses can be well explained. In this process, we consider some experimental results, such as the Higgs data of the discovered Higgs, B –physics measurements as well as precision electroweak measurements, to limit the parameter space, and plot the map of the profile likelihood (PL) for the excesses on different planes to study their implication on the model. In Section 4, we further study the constraints from the DM physics and the sparticle search, and point out that some explanations can easily survive the constraints. We also choose one parameter point to show that the fine tunings associated with the excesses are not serious. Conclusions are made in Section 5.

2 Theoretical preliminaries

2.1 NMSSM with the Type-I seesaw mechanism

As the simplest extension, the NMSSM with the Type-I seesaw mechanism augments the NMSSM by three generations of right-handed neutrino fields, and consequently it differs from the NMSSM only in neutrino/sneutrino sector. One ingenious byproduct is that the singlet Higgs field is responsible not only for μ problem, but also for extra neutrino

masses and sneutrino DM annihilation. With the field content presented in Table 1, the superpotential W and the soft breaking terms L_{soft} of the model are [47, 48]

$$\begin{aligned} W &= W_F + \lambda \hat{s} \hat{H}_u \cdot \hat{H}_d + \frac{1}{3} \kappa \hat{s}^3 + \bar{\lambda}_\nu \hat{s} \hat{\nu} + Y_\nu \hat{l} \cdot \hat{H}_u \hat{\nu}, \\ L_{\text{soft}} &= m_{H_d}^2 |H_d|^2 + m_{H_u}^2 |H_u|^2 + m_S^2 |S|^2 + \bar{m}_{\tilde{\nu}}^2 \tilde{\nu}_R \tilde{\nu}_R^* \\ &\quad + (\lambda A_\lambda S H_u \cdot H_d + \frac{1}{3} \kappa A_\kappa S^3 + \bar{\lambda}_\nu \bar{A}_{\lambda_\nu} S \tilde{\nu}_R^* \tilde{\nu}_R^* + Y_\nu A_\nu \tilde{\nu}_R^* \tilde{l} H_u + \text{h.c.}) + \dots \end{aligned} \quad (2.1)$$

where W_F denotes the superpotential of the MSSM without the μ term, and a \mathbb{Z}_3 symmetry is considered to forbid the appearance of any dimensional parameters in W . The coefficients λ and κ parameterize the interactions among the Higgs fields, and Y_ν and $\bar{\lambda}_\nu$ are neutrino Yukawa couplings with flavor index omitted to make the formula concise and more intuitive. Since the soft breaking squared masses $m_{H_u}^2$, $m_{H_d}^2$ and m_S^2 are related with the vacuum expectation values of the fields H_u , H_d and S , $\langle H_u \rangle = v_u/\sqrt{2}$, $\langle H_d \rangle = v_d/\sqrt{2}$ and $\langle S \rangle = v_s/\sqrt{2}$, by the minimization conditions of the Higgs potential after the electroweak symmetry breaking [24], it is customary to take λ , κ , $\tan \beta \equiv v_u/v_d$, A_λ , A_κ and $\mu \equiv \lambda v_s/\sqrt{2}$ as theoretical input parameters of the Higgs sector.

Same as the NMSSM, the extension predicts three CP-even Higgs mass eigenstates h_i ($i = 1, 2, 3$) with their mass matrix given by [30]

$$M_{11}^2 = \frac{2\mu(\lambda A_\lambda + \kappa\mu)}{\lambda \sin 2\beta} + (m_Z^2 - \frac{1}{2}\lambda^2 v^2) \sin^2 2\beta \quad (2.2)$$

$$M_{12}^2 = -\frac{1}{4}(2m_Z^2 - \lambda^2 v^2) \sin 4\beta \quad (2.3)$$

$$M_{13}^2 = -\sqrt{2}(\lambda A_\lambda + 2\kappa\mu) v \cos 2\beta \quad (2.4)$$

$$M_{22}^2 = m_Z^2 \cos^2 2\beta + 1/2 \lambda^2 v^2 \sin^2 2\beta \quad (2.5)$$

$$M_{23}^2 = \frac{v}{\sqrt{2}}[2\lambda\mu - (\lambda A_\lambda + 2\kappa\mu) \sin 2\beta] \quad (2.6)$$

$$M_{33}^2 = \frac{\lambda^2 v^2 A_\lambda \sin 2\beta}{4\mu} + \frac{\mu}{\lambda}(\kappa A_\kappa + 4\kappa^2 \frac{\mu}{\lambda}) \quad (2.7)$$

in the bases ($S_1 \equiv \cos \beta \text{Re}[H_u^0] - \sin \beta \text{Re}[H_d^0]$, $S_2 \equiv \sin \beta \text{Re}[H_u^0] + \cos \beta \text{Re}[H_d^0]$, $S_3 \equiv \text{Re}[S]$). Obviously, the basis S_2 represents the SM Higgs field and M_{22}^2 as its squared mass at tree level gets an additional contribution $1/2 \lambda^2 v^2 \sin^2 2\beta$ in comparison with corresponding MSSM prediction. The matrix also indicates that if the relation $M_{33}^2 < m_{22}^2$ holds, the mixing between S_2 and S_3 can further enhance the mass of the S_2 -dominated state. Benefiting from the contributions, the state does not need a large radiative contribution from stop loops to get its mass around 125 GeV [29–31]. Due to this attractive feature, this case was called natural NMSSM in literature [49]. The model also predicts two CP-odd mass eigenstates A_i ($i = 1, 2$), which are the mixtures of the imaginary parts of the fields H_u^0 , H_d^0 and S after removing the Goldstone degree of freedom, and a pair of charged Higgs bosons $H^\pm = \cos \beta H_u^\pm + \sin \beta H_d^\pm$. Throughout this paper, we label the neutral eigenstates in an ascending mass order, i.e. $m_{h_1} < m_{h_2} < m_{h_3}$ and $m_{A_1} < m_{A_2}$.

The Higgs sector of the model has following features:

- One CP-even state corresponds to the Higgs boson discovered at the LHC. Since experimental measurements require its property quite SM Higgs like, the mixing of the S_2 field with the other fields should be less than about 10% [3]. This implies from the definition of the S_1 and S_2 fields that it is $\text{Re}[H_u^0]$ dominated if $\tan\beta \gg 1$, and the heavy doublet-dominated state is mainly composed by $\text{Re}[H_d^0]$.
- Similar to the situation of the MSSM, the heavy doublet-dominated CP-even state is roughly degenerate in mass with the doublet-dominated CP-odd state, and also with the charged states. The LHC search for extra Higgs bosons together with the indirect constraints from B -physics have required $m_{H^\pm} \gtrsim 0.5\text{TeV}$ [50].
- With regard to the singlet-dominated states, they may be very light without conflicting with relevant collider constraints. One new function of these states is that they can couple directly with the sneutrino pair by three or four scalar interaction, which is induced by the $\bar{\lambda}_\nu \hat{s} \hat{\nu} \hat{\nu}$ term in the superpotential and its soft breaking term. As a result, they may appear as the final state of sneutrino pair annihilation in early universe or mediate the annihilation, and thus play an important role in DM physics.

Next we focus on DM physics in the Type-I seesaw extension of the NMSSM. In this framework, both the lightest $\tilde{\nu}_R$ -dominated sneutrino and the lightest neutralino can act as a viable DM candidate. A great advantage of the former candidate over the latter one is that, regardless the value of the Higgsino mass, the couplings of the sneutrino pair with SM particles are always small due to its singlet nature. This causes its scattering with nucleon suppressed greatly, and thus alleviates the constraints of DM DD experiments on the theory [43]. In the following, we only discuss the sneutrino DM case since it has much broader parameter space allowed by experiments.

For the neutrino/sneutrino sector, if one resorts the neutrino oscillations observed by different low energy experiments to the non-diagonality of the Yukawa coupling Y_ν , the soft breaking parameters such as $\bar{\lambda}_\nu$, $\bar{m}_{\tilde{\nu}}$ and \bar{A}_{λ_ν} can be flavor diagonal. In this case, the flavor mixings of the sneutrinos are extremely suppressed by the off-diagonal elements of Y_ν , and it is enough to only consider one generation sneutrinos in studying the properties of the sneutrino DM [43]. In our discussion, we assume the sneutrino DM carrying a τ flavor and use the symbols λ_ν , A_{λ_ν} and $m_{\tilde{\nu}}$ to denote the 33 elements of the matrix $\bar{\lambda}_\nu$, \bar{A}_{λ_ν} and $\bar{m}_{\tilde{\nu}}$ respectively. Moreover, due to the presence of lepton number violating interactions in the superpotential, the CP-even and -odd components of a sneutrino field are usually not degenerate in mass, and consequently the sneutrino DM has a definite CP number. For more details about the property of the sneutrinos (such as their mass form and field component), one can see the discussion in [43].

Possible annihilation channels of the sneutrino DM include [47, 48]

- (1) $\tilde{\nu}_1 \tilde{H} \rightarrow XY$ and $\tilde{H} \tilde{H}' \rightarrow X'Y'$ with \tilde{H} and \tilde{H}' denoting any Higgsino dominated neutralino or chargino and $X^{(\prime)}$ and $Y^{(\prime)}$ representing any lighter state. These annihilation channels are called coannihilation in literatures [45, 46], and they are important only when the mass splitting between \tilde{H} and $\tilde{\nu}_1$ is less than about 10%. As pointed

out by the Bayesian analysis of the model in [43], this channel is the most important annihilation mode.

- (2) $\tilde{\nu}_1 \tilde{\nu}_1 \rightarrow SS^*$ via the s -channel exchange of a Higgs boson, the t/u -channel exchange of a sneutrino, and any relevant scalar quartic couplings with S denoting a light Higgs boson. This is the second important annihilation channel of the DM.
- (3) $\tilde{\nu}_1 \tilde{\nu}_1 \rightarrow VV^*, VS, f\bar{f}$ with V and f denoting a vector boson (W or Z) and a SM fermion, respectively. This kind of annihilations proceeds via the s -channel exchange of a CP-even Higgs boson.
- (4) $\tilde{\nu}_1 \tilde{\nu}_1 \rightarrow \nu_R \bar{\nu}_R$ via the s -channel exchange of a Higgs boson and the t/u -channel exchange of a neutralino.
- (5) $\tilde{\nu}_1 \tilde{\nu}'_1 \rightarrow A_i^{(*)} \rightarrow XY$ and $\tilde{\nu}'_1 \tilde{\nu}'_1 \rightarrow X'Y'$ with $\tilde{\nu}'_1$ denoting a sneutrino with an opposite CP number to that of $\tilde{\nu}_1$. These annihilation channels are important in determining the relic density only when the CP-even and -odd states are nearly degenerate in mass.

The expressions of σv for some channels are presented in [48]. One can learn from them that the parameters in sneutrino sector, such as λ_ν , A_ν and $m_{\tilde{\nu}}^2$, as well as the parameters in the Higgs sector, are involved in the annihilations.

2.2 Formula for the $b\bar{b}$ and $\gamma\gamma$ signals

In the seesaw extension of the NMSSM, the singlet-dominated h_1 may account for the excesses. In order to illustrate this point, let's look at the analytic expression of the signal strength for the excesses in the narrow width approximation, which is given by

$$\begin{aligned}
\mu_{\text{LEP}}|_{m_{h_1} \simeq 96 \text{ GeV}} &= \frac{\sigma_{\text{SUSY}}(e^+e^- \rightarrow Zh_1)}{\sigma_{\text{SM}}(e^+e^- \rightarrow ZH)} \times \frac{\text{Br}_{\text{SUSY}}(h_1 \rightarrow b\bar{b})}{\text{Br}_{\text{SM}}(H \rightarrow b\bar{b})} \\
&\simeq |C_{h_1 VV}|^2 \times \frac{\Gamma_{\text{SUSY}}(h_1 \rightarrow b\bar{b})}{\Gamma_{\text{SUSY, tot}}} \times \frac{1}{0.799}, \\
\mu_{\text{CMS}}|_{m_{h_1} \simeq 96 \text{ GeV}} &= \frac{\sigma_{\text{CMS}}(pp \rightarrow h_1)}{\sigma_{\text{SM}}(pp \rightarrow h_1)} \times \frac{\text{Br}_{\text{SUSY}}(h_1 \rightarrow \gamma\gamma)}{\text{Br}_{\text{SM}}(h_1 \rightarrow \gamma\gamma)} \\
&\simeq |C_{h_1 gg}|^2 \times \frac{\Gamma_{\text{SUSY}}(h_1 \rightarrow \gamma\gamma)}{\Gamma_{\text{SUSY, tot}}} \times \frac{1}{1.43 \times 10^{-3}}, \tag{2.8}
\end{aligned}$$

where H denotes a SM Higgs boson with its mass at 96 GeV and its branching ratios given in [51], $\Gamma_{\text{SUSY, tot}} = \Gamma_{\text{SUSY}}(h_1 \rightarrow b\bar{b}) + \Gamma_{\text{SUSY}}(h_1 \rightarrow c\bar{c}) + \dots$ is the SUSY prediction on the total width of h_1 , and $C_{h_1 XX^*}$ ($X = b, g$) represents the coupling of h_1 with XX^* which is normalized to its SM prediction. Since current LHC data have required the properties of the discovered boson to highly mimic those of the SM Higgs boson and meanwhile colored sparticles heavier than about 1TeV, we have following approximation for the couplings

$$\begin{aligned}
C_{h_1 t\bar{t}} &\simeq -V_{11} \cot \beta + V_{12}, & C_{h_1 gg} &\simeq C_{h_1 t\bar{t}}, \\
C_{h_1 b\bar{b}} &\simeq V_{11} \tan \beta + V_{12}, & C_{h_1 VV} &= V_{12},
\end{aligned} \tag{2.9}$$

where V_{ij} with $i, j = 1, 2, 3$ denotes the element of the rotation matrix to diagonalize the mass matrix in Eq.(2.7). As for $C_{h_1\gamma\gamma}$, its expression is somewhat complex since besides the top quark- and W-mediated loops, it is also contributed by chargino loop and charged Higgs loop. To be more specific, although the charged Higgs loop is usually negligible since it is mediated by a heavy scalar particle [49], the chargino loop can play an important role in enhancing $\Gamma(h_1 \rightarrow \gamma\gamma)$ by [52]

$$\begin{aligned} C_{h_1\gamma\gamma}^{\tilde{\chi}^\pm} &\simeq \left(\frac{2}{9} A_{1/2}(\tau_t) - \frac{7}{8} A_1(\tau_W) \right)^{-1} \times \frac{\lambda v}{6|\mu|} \left(1 + \frac{7}{30} \frac{m_{h_1}^2}{4\mu^2} \right) V_{13} \\ &\simeq -1.37 \times \frac{\lambda v}{6|\mu|} \left(1 + \frac{7}{30} \frac{m_{h_1}^2}{4\mu^2} \right) V_{13} \quad \text{for } m_{h_1} = 96 \text{ GeV}, \end{aligned} \quad (2.10)$$

where $A_{1/2}$ and A_1 are loop functions with $\tau_i = m_i^2/(4m_i^2)$.

From these formula, one has following observations:

- If the theory is used to explain the excesses, the preferred mass spectrum is $m_{h_1} \simeq 96 \text{ GeV}$, $m_{h_2} \simeq 125 \text{ GeV}$ and $m_{h_3} \simeq m_{H^\pm} \gtrsim 500 \text{ GeV}$. Since the mass splitting between h_1 and h_3 is much larger than that between h_1 and h_2 , $V_{12} \gg V_{13}$ is kept for most cases. So one can conclude $C_{h_1VV} \simeq C_{h_1t\bar{t}} \simeq C_{h_1gg} \simeq V_{12}$ and $C_{h_1\gamma\gamma}^t + C_{h_1\gamma\gamma}^W \simeq V_{12}$ as an intuitive understanding.
- $C_{h_1b\bar{b}}$ may be significantly smaller than $C_{h_1t\bar{t}}$ due to the cancellation between its two contributions. In this case, $\Gamma_{\text{SUSY,tot}}$ is reduced greatly, but it does not change the fact that $h_1 \rightarrow b\bar{b}$ is the dominant decay channel of h_1 since the Yukawa coupling of h_1 with bottom quark is much larger than its couplings with the other light quarks and leptons.
- An uncertainty of 10% in C_{h_2VV} measurement by latest Higgs data at the LHC [3] implies that $|C_{h_1VV}|^2 \lesssim 0.2$. This size is large enough to produce the central value of the $b\bar{b}$ excess because $Br(h_1 \rightarrow b\bar{b})$ is insensitive to $C_{h_1b\bar{b}}$ if it is not suppressed too much.
- $C_{h_1\gamma\gamma}^{\tilde{\chi}^\pm}$ may be significant in comparison with the top- and W-loop contribution, e.g. $|C_{h_1\gamma\gamma}^{\tilde{\chi}^\pm}| > 0.1$ for $\lambda \gtrsim \frac{|\mu|}{550 \text{ GeV}}$, since $\mu \sim 100 \text{ GeV}$ is allowed in the theory by both the LHC search for sparticles and the DM experiments [43]. This fact together with a suppression of $C_{h_1b\bar{b}}$ (or equivalently $\Gamma_{\text{SUSY,tot}}$) can enhance $Br(h_1 \rightarrow \gamma\gamma)$ by several times in comparison with $Br_{\text{SM}}(h_1 \rightarrow \gamma\gamma)$ [53, 54], and consequently the diphoton excess can be explained.

3 Solutions to the excesses

In this section we attempt to find solutions to the excesses in the NMSSM with the Type-I seesaw mechanism. We utilize the package SARAH-4.11.0 [55–57] to build the model, the codes SPheno-4.0.3 [58] and FlavorKit [59] to generate particle spectrum and compute low

energy flavor observables respectively, and the package `HiggsBounds-5.3.2` [60] to implement the constraints from the direct search for extra Higgs bosons at LEP, Tevatron and LHC. For some benchmark settings, we also use the package `MicrOMEGAs 4.3.4` [62–64] to calculate DM observables by assuming the lightest sneutrino as the sole DM candidate in the universe. In calculating the radiative correction to the Higgs mass spectrum, the code `SPheno-4.0.3` only includes full one- and two-loop effects using a diagrammatic approach with vanishing external momenta [58]. This leaves an uncertainty of about 2 GeV for the SM-like Higgs boson mass.

3.1 Strategy in scanning the parameter space

Previous discussions indicate that only the parameters in the Higgs sector determine the $b\bar{b}$ and $\gamma\gamma$ signals. We perform a sophisticated scan over these inputs and the soft trilinear coefficient A_t for top squark (since this parameter can affect significantly the Higgs mass spectrum by radiative correction) in following ranges²

$$\begin{aligned} 0 < \lambda \leq 0.75, \quad 0 < \kappa \leq 0.75, \quad 1 \leq \tan \beta \leq 20, \quad 100 \text{ GeV} \leq \mu \leq 600 \text{ GeV}, \\ 300 \text{ GeV} \leq A_\lambda \leq 2\text{TeV}, \quad -1\text{TeV} \leq A_\kappa \leq 0\text{TeV}, \quad |A_t| \leq 5\text{TeV}, \end{aligned} \quad (3.1)$$

where all the parameters are defined at the scale $Q = 1\text{TeV}$. The other unimportant parameters are set as follows: $\lambda_\nu = 0.1$, $M_1 = M_2 = 2\text{TeV}$ and $M_3 = 5\text{TeV}$ for gaugino soft breaking masses, and all soft breaking parameters in squark and slepton sectors except A_t are fixed at 2TeV, which are consistent with the results of the LHC search for sparticles. In the scan, we adopt the MultiNest algorithm in [65] with the flat distribution for the inputs and $n\text{live} = 10000$ ³, and construct the likelihood function

$$\chi^2 = \chi_{\text{excess}}^2 + \chi_{h_{2,\text{mass}}}^2, \quad (3.2)$$

$$\mathcal{L} = \mathcal{L}_{\text{excess}} \times \mathcal{L}_{h_{2,\text{mass}}} \equiv \text{Exp} \left[-\frac{1}{2} \chi^2 \right], \quad (3.3)$$

to guide the scan where χ_{excess}^2 and $\chi_{h_{2,\text{mass}}}^2$ are the χ^2 function of the excesses and m_{h_2} respectively with their forms given by⁴

$$\begin{aligned} \chi_{\text{excess}}^2 &= \left(\frac{m_{h_1} - 96.0}{0.2} \right)^2 + \left(\frac{\mu_{\text{LEP}} - 0.117}{0.057} \right)^2 + \left(\frac{\mu_{\text{CMS}} - 0.6}{0.2} \right)^2, \\ \chi_{h_{2,\text{mass}}}^2 &= \left(\frac{m_{h_2} - 125.1}{2.0} \right)^2. \end{aligned} \quad (3.4)$$

In the scan, we also calculate following χ^2 functions for each sample

²Note that we are not intend to perform a complete fit of the model to the excesses in this work, so we only select by experience part of its parameter space for study.

³The setting *nlive* in the MultiNest method denotes the number of active or live points used to determine the iso-likelihood contour in each iteration [65, 66]. The larger it is, the more meticulous the scan becomes in surveying the parameter space.

⁴We assume relatively small total (theoretical and experimental) uncertainties for m_{h_1} and m_{h_2} in the study, i.e. $\Delta m_{h_1} = 0.2 \text{ GeV}$ and $\Delta m_{h_2} = 2 \text{ GeV}$, to ensure that the samples obtained in the scan focus on the case $m_{h_1} \simeq 96 \text{ GeV}$ and $m_{h_2} \simeq 125 \text{ GeV}$. Moreover, we do not include the coupling information of the discovered Higgs boson in the \mathcal{L} because we want to get the best solutions to the excess instead of to perform a global fit of the model with all experimental data.

- $\chi_{h_2, \text{couplings}}^2$ for seven couplings of the discovered Higgs boson in the κ -framework, which were recently obtained by ATLAS collaboration with 80 fb^{-1} data. We use the results of the couplings and their correlation matrix in Table 11 and Figure 38 of [3] respectively to calculate the $\chi_{h_2, \text{couplings}}^2$. We do not include the theoretical uncertainty in calculating the couplings since they are much smaller than corresponding experimental uncertainty.
- χ_B^2 for the measurement of $Br(B \rightarrow X_s \gamma)$ and $Br(B_s \rightarrow \mu^+ \mu^-)$, which takes the form [67]

$$\chi_B^2 = \frac{(B_\gamma - 3.43)^2}{0.4^2} + \frac{(B_{\mu^+ \mu^-} - 3.11)^2}{1.2^2}$$

with B_γ and $B_{\mu^+ \mu^-}$ denoting the theoretical prediction of $Br(B \rightarrow X_s \gamma)$ and $Br(B_s \rightarrow \mu^+ \mu^-)$ in unit of 10^{-4} and 10^{-9} , respectively.

- χ_{EW}^2 for precision electroweak measurements ϵ_i ($i = 1, 2, 3$) [68–70] or equivalently S , T and U parameters [71, 72]. We use the formula for the self-energies of the gauge bosons γ , W^\pm and Z in [73] to calculate these observables, and the fit results in [74] to get the χ_{EW}^2 .

In getting the solutions to the excesses, we only consider the samples in the scan that survive the constraints from the **HiggsBounds**, satisfy $m_{A_1} > m_{h_2}/2$ so that the discovered Higgs boson has no exotic decay and meanwhile $\chi_{\text{tot}}^2 \leq 18.6$ with χ_{tot}^2 defined by⁵

$$\chi_{\text{tot}}^2 = \chi_{\text{excess}}^2 + \chi_{h_2, \text{mass}}^2 + \chi_{h_2, \text{couplings}}^2 + \chi_B^2 + \chi_{\text{EW}}^2. \quad (3.5)$$

At this stage, we remind that, if one does not consider the constraints from DM physics and relevant sparticle searches at the LHC, the Higgs physics of the NMSSM is same as that of the extended model. So one may also use the package **NMSSMTools** [75, 76] to perform the scan. We compare the **NMSSMTools** with our toolkit, and find that their solutions to the excesses shown in following figures are similar, although the **NMSSMTools** is somewhat faster than our toolkit in calculation.

3.2 Numerical Results

Based on the samples obtained in the scan, we plot the profile likelihoods (PL) of \mathcal{L} in Eq.(3.3) on different planes⁶, where the color bar in Fig.1, 2 and 3 represents the PL value

⁵ χ_{tot}^2 denotes a measure of the agreement between the theory and the total experimental data considered in this work. In this hypothesis, the goodness-of-fit measure χ_{tot}^2 obeys a χ^2 distribution with $N_{\text{obs}} - N_{\text{para}} + 1$ degree of freedom (d.o.f.). In our study, the d.o.f. is $16 - 7 + 1 = 10$, and $\chi_{\text{tot}}^2 = 18.6$ corresponds to the upper limit of χ_{tot}^2 at 2σ confidence level.

⁶The frequentist PL is defined as the largest likelihood value in a certain parameter space [77]. Given a likelihood function \mathcal{L} defined in N -dimensional space $\Theta = (\Theta_1, \Theta_2, \dots, \Theta_N)$, its two dimensional PL can be obtained by the procedure

$$\mathcal{L}(\Theta_i, \Theta_j) = \max_{\Theta_1, \dots, \Theta_{i-1}, \Theta_{i+1}, \dots, \Theta_{j-1}, \Theta_{j+1}, \dots, \Theta_N} \mathcal{L}(\Theta).$$

Obviously, the PL reflects the preference of a theory on the parameter space, and for a given point on $\Theta_i - \Theta_j$ plane, the value of $\mathcal{L}(\Theta_i, \Theta_j)$ represents the capability of the point in the theory to account for experimental data by varying the other parameters.

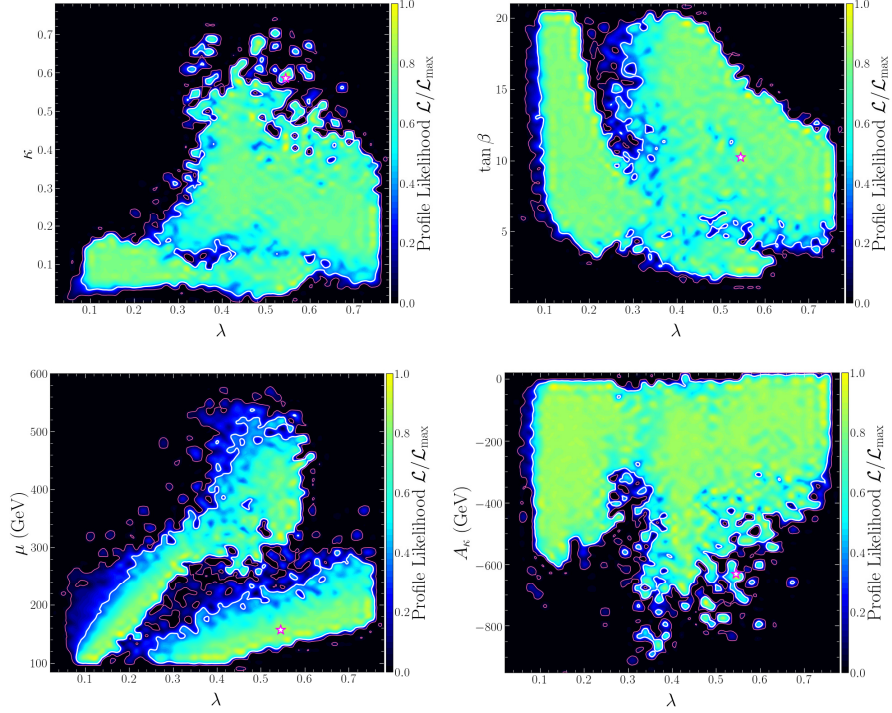


Figure 1. Two dimensional profile likelihood of \mathcal{L} in Eq.(3.3), which are projected on $\kappa - \lambda$, $\tan \beta - \lambda$, $\mu - \lambda$ and $A_\kappa - \lambda$ planes respectively. Since $\chi^2_{\min} \simeq 0$ for the best point (marked by star symbol in the figure), the 1σ boundary (white solid line) and the 2σ boundary (red line) correspond to $\chi^2 \simeq 2.3$ and $\chi^2 \simeq 6.18$, respectively. This figure reflects the preference of the excesses on the parameter space of the extended NMSSM.

relative to the best point marked by star symbol, and the white and pink solid lines are boundaries for 1σ and 2σ confidence intervals (CI), respectively. Fig.1 indicates that there are broad parameter space to interpret the excesses and the large deviation between the 1σ and 2σ boundaries on $\mu - \lambda$ plane reflects that the interpretation is sensitive to the parameters λ and μ . Fig.2 shows that the magnitude of the normalized couplings may reach 0.5 except $|C_{h_1 b\bar{b}}|$ which is relatively suppressed. The best point for the excesses predicts $C_{h_1 VV} = -0.36$, $C_{h_1 gg} = -0.41$, $C_{h_1 \gamma\gamma} = -0.48$, $C_{h_1 t\bar{t}} = -0.36$ and $C_{h_1 b\bar{b}} = 0.24$, and consequently $Br(h_1 \rightarrow b\bar{b}) = 73\%$ and $Br(h_1 \rightarrow \gamma\gamma) = 0.5\%$. The pattern $Br(h_1 \rightarrow b\bar{b})/Br_{\text{SM}}(H \rightarrow b\bar{b}) < 1$ and $Br(h_1 \rightarrow \gamma\gamma)/Br_{\text{SM}}(H \rightarrow \gamma\gamma) \simeq 3.7$ agrees well with the expectation in section II. Moreover, a closer analysis of the samples reveals that the interpretation is distributed in three isolated parameter regions

- **Region I:** $0.06 \lesssim \lambda \lesssim 0.37$, $0.03 \lesssim \kappa \lesssim 0.2$, $4 \lesssim \tan \beta \lesssim 20$, $100 \text{ GeV} \lesssim \mu \lesssim 350 \text{ GeV}$ and $\lambda/\mu \sim 1/800 \text{ GeV}$,
- **Region II:** $0.22 \lesssim \lambda \lesssim 0.75$, $0.05 \lesssim \kappa \lesssim 0.7$, $4 \lesssim \tan \beta \lesssim 20$, $100 \text{ GeV} \lesssim \mu \lesssim 300 \text{ GeV}$ and $\lambda/\mu \sim 1/250 \text{ GeV}$,
- **Region III:** $0.37 \lesssim \lambda \lesssim 0.56$, $0.01 \lesssim \kappa \lesssim 0.15$, $2 \lesssim \tan \beta \lesssim 5$ and $250 \text{ GeV} \lesssim \mu \lesssim 560 \text{ GeV}$,

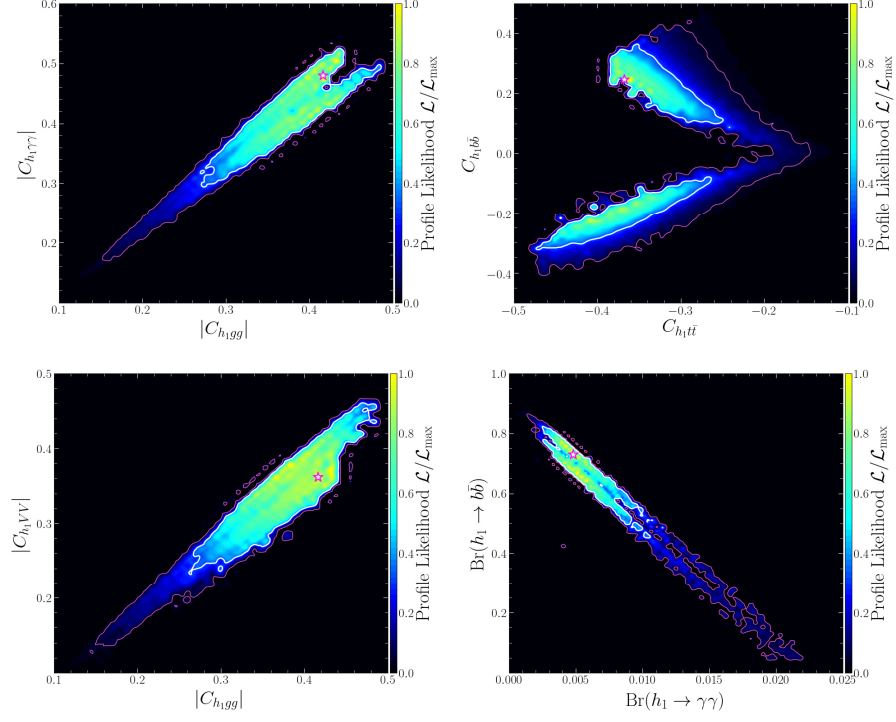


Figure 2. Similar to Fig.1, but projected on $|C_{h_1\gamma\gamma}| - |C_{h_1gg}|$, $C_{h_1b\bar{b}} - C_{h_1t\bar{t}}$, $|C_{h_1VV}| - |C_{h_1gg}|$ and $Br(h_1 \rightarrow \gamma\gamma) - Br(h_1 \rightarrow b\bar{b})$ planes, respectively.

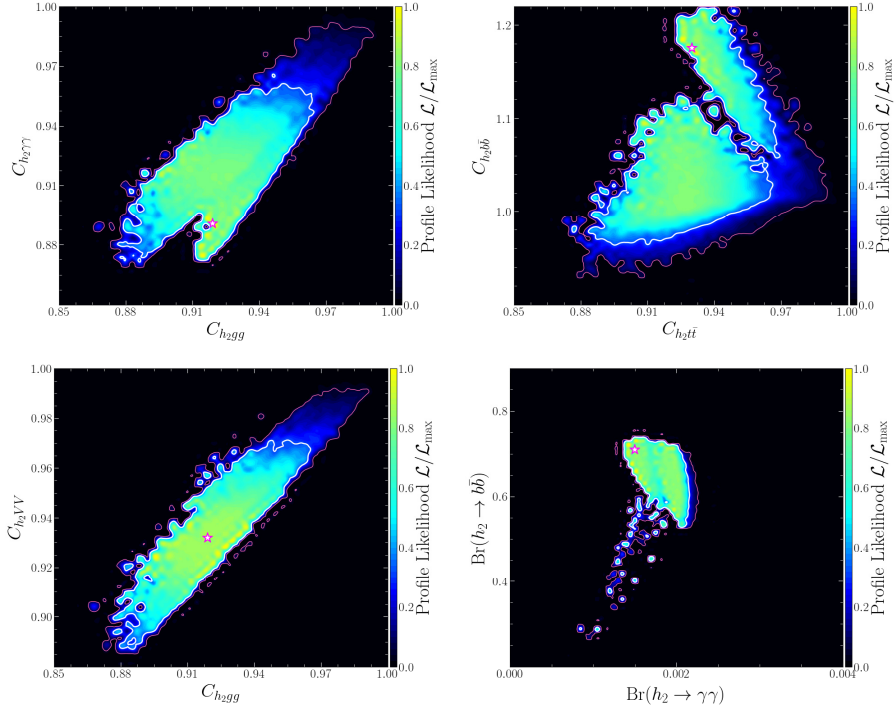


Figure 3. Similar to Fig.1, but projected on $C_{h_2\gamma\gamma} - C_{h_2gg}$, $C_{h_2b\bar{b}} - C_{h_2t\bar{t}}$, $C_{h_2VV} - C_{h_2gg}$ and $Br(h_2 \rightarrow \gamma\gamma) - Br(h_2 \rightarrow b\bar{b})$ planes, respectively.

λ	κ	$\tan \beta$	μ	A_κ	A_λ	A_t	m_{h_1}	m_{h_2}	m_{h_3}
0.164	0.112	19.24	147.7	-304.6	1785.0	1354.7	95.9	124.6	2332.9
$m_{\tilde{\chi}_1^0}$	$m_{\tilde{\chi}_2^0}$	$m_{\tilde{\chi}_1^\pm}$	μ_{CMS}	μ_{LEP}	$\chi_{h_2, \text{couplings}}^2$	Z_{11}	Z_{12}	Z_{13}	Z_{22}
145.1	155.8	152.9	0.5882	0.1186	7.62	0.01	0.39	-0.92	-0.92

Table 2. Benchmark setting of the **Region I** with dimensional parameters in unit of GeV.

and they are characterized by

- The posterior probabilities of the three regions are 0.80, 0.16 and 0.04 respectively⁷. This reflects the fact that the **Region I** is more likely to explain the excesses.
- In both the **Region I** and the **Region II**, the lightest neutralino $\tilde{\chi}_1^0$ may be either Higgsino-dominated or Singlino-dominated (corresponding to $2\kappa/\lambda > 1$ and $2\kappa/\lambda < 1$ respectively [24]), while in the **Region III**, $\tilde{\chi}_1^0$ is only Singlino dominated.
- All the regions are able to predict the central value of the excesses. In the **Region I** and the **Region III**, the most favored parameter points predict $\chi_{h_2, \text{couplings}}^2 \sim 7$, while those in the **Region II** usually predict $\chi_{h_2, \text{couplings}}^2 > 10$. This fact reflects that there is minor tension between the excesses and the data of the discovered Higgs for the **Region II**.
- The **Region I** (**Region II**) corresponds to the lower branch (upper branch) of the panel a in Fig.2. For both the branches, V_{12} in Eq.(2.10) is always negative, and $C_{h_1 b\bar{b}}$ may be either negative (the lower branch) or positive (the upper branch) due to the moderate (strong) cancellation between $V_{11} \tan \beta$ and V_{12} in the expression of $C_{h_1 b\bar{b}}$. This conclusion applies to the panels b and c in Fig.2.
- For all the regions, $m_{H^\pm} \gtrsim 550$ GeV which is consistent with the results in [21] for a general NMSSM, and A_1 may be lighter than 100 GeV.

We also study the couplings of the SM-like Higgs boson in Fig.3. This figure shows that the normalized couplings $C_{h_2 VV}$, $C_{h_2 \gamma\gamma}$, $C_{h_2 gg}$ and $C_{h_2 t\bar{t}}$ is centered around 0.92, and $C_{h_2 b\bar{b}}$ may reach 1.2. $Br(h_2 \rightarrow b\bar{b})$ varies from 0.55 to 0.75 in comparison with its SM prediction 0.575 ± 0.018 , and $Br(h_2 \rightarrow \gamma\gamma)$ changes from 1.3×10^{-3} to 2.2×10^{-3} with its SM prediction $(2.28 \pm 0.11) \times 10^{-3}$ [51]. As pointed out in [17], the sizable deviation of the couplings from its SM predictions and the presence of h_1 can be explored by future high luminosity LHC or e^+e^- colliders.

⁷The concept of the posterior probability comes from Bayesian theorem, which was briefly introduced in [77].

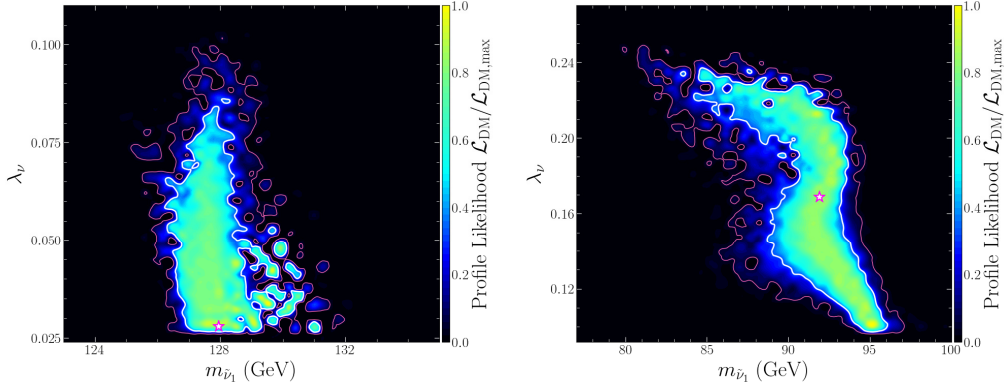


Figure 4. The map for the profile likelihood of \mathcal{L}_{DM} in Eq.(4.3), which is plotted on $\lambda_\nu - m_{\tilde{\nu}_1}$ plane. Given that $\chi^2_{\text{DM,min}} \simeq 0$ for the best point which is marked by star symbol, the 1σ boundary (white solid line) and the 2σ boundary (red line) correspond to $\chi^2_{\text{DM}} \simeq 2.3$ and $\chi^2_{\text{DM}} \simeq 6.18$, respectively. The left panel is for the setting of the **Region I**, and the right panel is for the setting of the **Region II**.

λ	κ	$\tan\beta$	μ	A_κ	A_λ	A_t	m_{h_1}	m_{h_2}	m_{h_3}
0.355	0.433	15.66	115.9	-502.1	1319.1	-1901.5	96.1	125.1	1623.7
$m_{\tilde{\chi}_1^0}$	$m_{\tilde{\chi}_2^0}$	$m_{\tilde{\chi}_1^\pm}$	μ_{CMS}	μ_{LEP}	$\chi^2_{h_2, \text{couplings}}$	Z_{11}	Z_{12}	Z_{13}	Z_{22}
109.1	126.5	119.7	0.547	0.088	9.0	0.01	-0.32	0.95	0.95

Table 3. Same as Table 2, but for the benchmark setting of the **Region II**.

4 Constraints from DM physics and sparticle search

So far we do not consider the constraints from DM physics and the LHC search for sparticles on the regions. For each sample obtained from the scan in last section, these constraints can be implemented by following procedures [43]:

- Vary the parameters λ_ν , A_{λ_ν} and $m_{\tilde{\nu}}$ in the sneutrino sector, and select the sample for which the lightest sneutrino is the lightest sparticle of the theory and the decay channel $h_1 \rightarrow \nu_R \bar{\nu}_R$ (ν_R denotes a right-handed neutrino) is kinematically forbidden. Since $m_{\nu_R} = 2\lambda_\nu \mu / \lambda$, the latter requirement is equivalent to

$$\lambda_\nu \gtrsim \lambda \times \frac{24 \text{ GeV}}{\mu}. \quad (4.1)$$

- Take the sneutrino as a sole DM candidate, calculate DM quantities such as its relic density, its scattering rate with nucleon and the photon spectrum of its annihilation in dwarf galaxy, and compare them with relevant measurements of the Planck experiment, the XENON-1T experiment and the Fermion-LAT experiment, respectively.
- Study the signals of electroweakino production processes at the LHC, and check by simulations whether the signals coincide with the LHC results.

Since the involved calculations are rather complex and meanwhile more than 0.1 million samples were accumulated in the scan, it is very time consuming to check all the samples by the constraints. Instead, we only consider one benchmark setting for each of the three regions and illustrate its underlying physics.

Let's first consider the benchmark setting of the **Region I**, whose information is presented in Table 2. We perform a further scan over following region

$$0 < m_\nu < 150 \text{ GeV}, \quad 0 < \lambda_\nu < 0.5, \quad |A_{\lambda_N}| < 1 \text{ TeV}, \quad (4.2)$$

with the **MultiNest** algorithm by requiring $m_{\nu_R} > m_{h_1}/2$ and assuming the sneutrino DM to be CP-even with τ flavor. The likelihood function we adopt is composed by

$$\mathcal{L}_{\text{DM}} = \mathcal{L}_{\Omega_{\tilde{\nu}_1}} \times \mathcal{L}_{\text{DD}} \times \mathcal{L}_{\text{ID}}, \quad (4.3)$$

where $\mathcal{L}_{\Omega_{\tilde{\nu}_1}}$, \mathcal{L}_{DD} and \mathcal{L}_{ID} account for the relic density, the XENON-1T experiment and the Fermi-LAT observation of dwarf galaxy respectively, and their explicit forms are presented in [43]. In the left panel of Fig.4, we present the profile likelihood of \mathcal{L}_{DM} for the setting in Table 2 on $\lambda_\nu - m_{\tilde{\nu}_1}$ plane with $m_{\tilde{\nu}_1}$ denoting the DM mass. This panel shows that the mass of $\tilde{\nu}_1$ is roughly degenerate with the Higgsino mass μ , which implies that the DM gets the right relic density through co-annihilating with the Higgsinos [43]. Given that $\tilde{\chi}_1^0$ and $\tilde{\chi}_2^0$ in this setting decay by $\tilde{\chi}_{1,2}^0 \rightarrow \nu_\tau \tilde{\nu}_1$ and thus they correspond to missing momentum at the LHC, the most promising channel to probe the Higgsinos is through the process $pp \rightarrow \tilde{\chi}_1^\pm \tilde{\chi}_1^\mp \rightarrow (\tau^\pm \tilde{\nu}_1)(\tau^\mp \tilde{\nu}_1)$ [43]. Obviously, the LHC has no capability to exclude the moderately light Higgsinos since the τ leptons are soft due to the compressed mass spectrum of $\tilde{\chi}_1^\pm$ and $\tilde{\nu}_1$ [43]. The panel also shows that λ_ν is upper bounded by about 0.1, which means that the DM can not annihilate by the channel $\tilde{\nu}_1 \tilde{\nu}_1 \rightarrow h_1 h_1$ to get its right relic density (see the formula of the relic density in various simple DM theories [78, 79]). This is mainly due to the constraint from DM DD experiments, which may be understood as follows: in the seesaw extension of the NMSSM, the $\tilde{\nu}_1$ -nucleon scattering proceeds mainly by exchanging CP-even Higgs bosons, so any large $\tilde{\nu}_1 \tilde{\nu}_1 h_1$ and/or $\tilde{\nu}_1 \tilde{\nu}_1 h_2$ couplings are dangerous to spoil the XENON-1T bound. For a CP-even $\tilde{\nu}_1$, the coupling strength is given by [43]

$$C_{\tilde{\nu}_1 \tilde{\nu}_1 h_i} = \frac{\lambda \lambda_\nu M_W}{g} (\sin \beta Z_{i1} + \cos \beta Z_{i2}) - \left[\frac{\sqrt{2}}{\lambda} (2\lambda_\nu^2 + \kappa \lambda_\nu) \mu - \frac{\lambda_\nu A_{\lambda_\nu}}{\sqrt{2}} \right] Z_{i3}, \quad (4.4)$$

with Z_{ij} ($i, j = 1, 2, 3$) corresponding to the elements of the matrix to diagonalize the CP-even Higgs mass matrix in the basis $(\text{Re}[H_d^0], \text{Re}[H_u^0], \text{Re}[S])$ and their values given in Table 2 for the setting. With regard to the specific setting, $C_{\tilde{\nu}_1 \tilde{\nu}_1 h_1}/\lambda_\nu$ is contributed mainly by the second bracket in Eq.(4.4), and it is quite large (exceeding 200 GeV) because $\mu/\lambda \sim 900$ GeV and A_{λ_ν} is negative⁸. The situation of $C_{\tilde{\nu}_1 \tilde{\nu}_1 h_2}/\lambda_\nu$ is quite similar since $|Z_{23}| = 0.39$ is not a small number, and more importantly h_1 and h_2 are constructive in

⁸As shown by the sneutrino mass matrix in [43], a negative A_{λ_ν} is needed to ensure that a CP-even sneutrino state is lighter than its CP-odd partner.

λ	κ	$\tan\beta$	μ	A_κ	A_λ	A_t	m_{h_1}	m_{h_2}	m_{h_3}
0.434	0.091	5.06	317.7	-175.3	1467.1	-1967.1	96.1	125.3	1595.2
$m_{\tilde{\chi}_1^0}$	$m_{\tilde{\chi}_2^0}$	$m_{\tilde{\chi}_1^\pm}$	μ_{CMS}	μ_{LEP}	$\chi_{h_2, \text{couplings}}^2$	Z_{11}	Z_{12}	Z_{13}	Z_{22}
133.4	330.4	324.0	0.694	0.1055	7.52	0.04	0.38	-0.92	-0.90

Table 4. Same as Table 2, but for the benchmark setting of the **Region III**.

contributing to the scattering cross section (for the complete expression of the cross section, see [43]). So in order to survive the XENON-1T constraint, λ_ν must be upper bounded by about 0.1 and correspondingly the co-annihilation channel is dominant. This usually predicts the SI cross section varying from 10^{-48} cm^2 to 10^{-47} cm^2 , and only in some rare cases it may be below 10^{-50} cm^2 . We checked that this conclusion also applies to the case of a CP-odd sneutrino DM, where, although A_{λ_ν} may be either positive or negative to get a CP-odd sneutrino DM [43], its magnitude is limited so that it can not cancel the contribution of the $\sqrt{2}\mu(2\lambda_\nu^2 + \kappa\lambda_\nu)/\lambda$ term in an efficient way.

Next we turn to the setting of the **Region II** in Table 3, which is featured by $\mu/\lambda \simeq 326 \text{ GeV}$ and $\lambda_\nu \gtrsim 0.08$. Similar to what we did for the **Region I**, we plot the profile likelihood on $\lambda_\nu - m_{\tilde{\nu}_1}$ plane, and show the boundaries of 1σ CI (white solid line) and 2σ CI (red line) on the right panel of Fig.4. We find that the samples in the 2σ CI annihilated mainly by the channel $\tilde{\nu}_1\tilde{\nu}_1 \rightarrow h_1h_1$ in early universe. This annihilation requires $\lambda_\nu \sim 0.15$ to get the right relic density [78, 79], and due to the temperature effect, $\tilde{\nu}_1$ may be lighter than h_1 in proceeding the annihilation [46]. We also find that the samples predict the scattering cross section ranging from 10^{-52} cm^2 to $3 \times 10^{-47} \text{ cm}^2$, so the constraints from current DM DD experiments is rather weak. Same as the previous setting, the Higgsinos may be probed by the process $pp \rightarrow \tilde{\chi}_1^\pm \tilde{\chi}_1^\mp \rightarrow (\tau^\pm \tilde{\nu}_1)(\tau^\mp \tilde{\nu}_1)$. From the simulation results in [43], the regions of $\mu \lesssim 170 \text{ GeV}$ and $\mu \gtrsim 280 \text{ GeV}$ can survive the LHC constraints for the DM mass given in the panel.

Finally we consider the benchmark setting of the **Region III** in Table 4. Different from the other settings, $\tilde{\chi}_1^0$ is now Singlino dominated and $\tilde{\nu}_1$ is unlikely to co-annihilate with it to get right relic density because the couplings of $\tilde{\chi}_1^0$ with SM particles are rather weak. Since the relic density requires $\lambda_\nu \gtrsim 0.1$ when the DM annihilated mainly by $\tilde{\nu}_1\tilde{\nu}_1 \rightarrow h_1h_1$ and meanwhile $\tan\beta$ is relatively small, the h_2 mediated contribution to $\sigma_{\tilde{\nu}_1-p}^{\text{SI}}$ is significantly large. This results in $\sigma_{\tilde{\nu}_1-p}^{\text{SI}} \gtrsim 1 \times 10^{-47} \text{ cm}^2$ for most cases, and only in some corners of the space in Eq.(4.2) can the setting survive the XENON-1T bound. On the other side, the Higgsino dominated $\tilde{\chi}_{2,3}$ decay by the channel $\tilde{\chi}_{2,3}^0 \rightarrow Z\tilde{\chi}_1^0, h_1\tilde{\chi}_1^0, h_2\tilde{\chi}_1^0, A_1\tilde{\chi}_1^0$ with $\tilde{\chi}_1^0 \rightarrow \tilde{\nu}_1\nu_\tau$, and they may be detected through the process $pp \rightarrow \tilde{\chi}_{2,3}\tilde{\chi}_1^\pm \rightarrow Z^{(*)}W^{(*)}2\tilde{\chi}_1^0$ by tri-lepton plus E_T^{miss} signal. For the setting in Table 4, we calculate the R value of the signal by the analysis of CMS collaboration with 35.9 fb^{-1} data [80]⁹, like what we did

⁹Note that the CMS analysis of the multi-lepton signal with 35.9 fb^{-1} [80] is slightly stronger than corresponding ATLAS analysis with 139 fb^{-1} data [81] in limiting the electroweakinos when $\mu \lesssim 300 \text{ GeV}$.

Region		DM Annihilation	DM DD Constraint	LHC Signal
Region I	$\frac{2\kappa}{\lambda} > 1$	$\tilde{\nu}_1 \tilde{H}$ co-annihilation	Weak	soft $2\tau + E_T^{\text{miss}}$
	$\frac{2\kappa}{\lambda} < 1$	$\tilde{\nu}_1 \tilde{\nu}_1 \rightarrow h_1 h_1$	Strong	$W^{(*)} Z^{(*)} + E_T^{\text{miss}}$
Region II	$\frac{2\kappa}{\lambda} > 1$	$\tilde{\nu}_1 \tilde{\nu}_1 \rightarrow h_1 h_1$	Weak	$2\tau + E_T^{\text{miss}}$
	$\frac{2\kappa}{\lambda} < 1$	$\tilde{\nu}_1 \tilde{\nu}_1 \rightarrow h_1 h_1$	Weak	$W^{(*)} Z^{(*)} + E_T^{\text{miss}}$
Region III	$\frac{2\kappa}{\lambda} < 1$	$\tilde{\nu}_1 \tilde{\nu}_1 \rightarrow h_1 h_1$	Moderately strong	$W^{(*)} Z^{(*)} + E_T^{\text{miss}}$

Table 5. Summary of the DM physics and the LHC signals for the **Region I, II, III** discussed in the text.

in [34]. We find $R = 0.68$ given $Br(\tilde{\chi}_2^0 \rightarrow Z\tilde{\chi}_1^0) = 32\%$ and $Br(\tilde{\chi}_3^0 \rightarrow Z\tilde{\chi}_1^0) = 76\%$ in the setting¹⁰. In fact, we also consider several other points in the region, and we find that they survive the LHC constraints mainly due to the suppression of $Br(\tilde{\chi}_{2,3}^0 \rightarrow Z\tilde{\chi}_1^0)$. Since these points predicts $R > 0.5$, they may be detected by future LHC experiment.

Before we end this section, we have more explanations:

- All the three benchmark settings can explain well the excesses and meanwhile keep consistent with the constraints from the DM physics and the LHC search for the electroweakinos by choosing appropriate λ_ν , A_{λ_ν} and $m_{\tilde{\nu}}$. Especially, the constraints are rather weak for the **Region I** when $2\kappa/\lambda > 1$ and the co-annihilation is responsible for the relic density.
- For both the **Region I** and the **Region II**, $2\kappa/\lambda$ may be less than 1. This situation is quite similar to that of the **Region III** where $\tilde{\chi}_1^0$ is Singlino dominated and λ_ν must be larger than 0.1 to get right relic density. Then from our previous discussion about the **Region I** and the **Region II**, one can infer that the **Region I** has been tightly limited by DM DD experiments, while the **Region II** is still allowed. We checked the correctness of this conclusion. Moreover, the best way to detect the Higgsinos is through the process $pp \rightarrow \tilde{\chi}_{2,3}^0 \tilde{\chi}_1^\pm \rightarrow Z^{(*)} W^{(*)} 2\tilde{\chi}_1^0$, and the tri-lepton signal is usually suppressed due to the open up of the decay channels $\tilde{\chi}_{2,3}^0 \rightarrow h_1 \tilde{\chi}_1^0, h_2 \tilde{\chi}_1^0, A_1 \tilde{\chi}_1^0$. This feature is helpful for the samples in these regions to escape the LHC constraint.

In Table 5, we summarize the DM physics and the LHC signal of the three regions, which may serve as a guideline to pick out good solutions to the excesses. We also choose a benchmark point for the setting in Table 2, which sets $\lambda_\nu = 0.045$, $A_{\lambda_\nu} = -201.8$ GeV and $m_{\tilde{\nu}} = 133.7$ GeV, and consequently predicts $\Omega h^2 = 0.1243$ and $\sigma_{\tilde{\nu}_1-p}^{\text{SI}} = 1.6 \times 10^{-47}$ cm², and calculate its theoretical fine tunings to predict some measurements. We get $\Delta_Z = 6.37$, $\Delta_{m_{h_1}} = 12.95$, $\Delta_{m_{h_2}} = 62.2$, $\Delta_{\Omega h^2} = 20.2$, $\Delta_{\sigma_{\tilde{\nu}_1-p}^{\text{SI}}} = 8.58$, $\Delta_{\mu_{\text{CMS}}} = 6.16$ and $\Delta_{\mu_{\text{LEP}}} =$

¹⁰ $R \equiv s/s_{95}^{\text{obs}}$ is the ratio of theoretical prediction of the signal to its experimental observed 95% C.L. upper limit, therefore $R > 1$ indicates that the theoretical prediction contradicts experimental observation. For more details about the calculation of R , see our previous works [34, 43].

20.65. In the calculation, we adopt the definition of Δ_Z and Δ_{h_i} ($i = 1, 2, 3$) from [82] and [83] with the input parameters set at the electroweak scale. As for the last four fine tunings, they are obtained by maximizing the ratio $\partial \ln O / \partial \ln p_i$ over the input parameter p_i in Eq.(3.1) and Eq.(4.2) with O denoting an observable. These results indicate that the solutions to the excesses in the seesaw extension is quite natural and thus deserves a careful study.

5 Conclusions

The discovery of the SM-like Higgs boson at the LHC validates the Higgs mechanism, while the deficiencies in the Higgs sector of the SM imply a more complex structure to account for the EWSB. The long standing $b\bar{b}$ excess at LEP-II and the continuously observed $\gamma\gamma$ excess by CMS collaboration provide potentially useful hints about the EWSB, and thus they deserve a careful study in new physics models.

In this work we show by both analytic formulas and numerical results that the NMSSM with the Type-I seesaw mechanism can naturally predict the central values of the excesses in its broad parameter space, and the solutions are consistent with the Higgs data of the discovered Higgs boson, B -physics and DM physics measurements, the electroweak precision data as well as the LHC search for sparticles. This great capability of the theory basically comes from the relaxation of the DM DD constraints. Explicitly speaking, the seesaw mechanism augments the NMSSM by three generations of right-handed neutrino fields, and renders the lightest sneutrino as a viable DM candidate. Due to the gauge singlet nature of the DM, its scattering with nucleon is suppressed in most cases to coincide spontaneously with the latest XENON-1T results. Consequently, broad parameter spaces in the Higgs sector, especially a light Higgsino mass, are resurrected as experimentally allowed, which makes the theory well suited to explain the excesses.

Our results indicate that the scalar responsible for the excesses should contain a sizable component of the SM Higgs field, and its decay branching ratio into $\gamma\gamma$ state is preferred several times larger than corresponding SM prediction to account for the excesses. The latter can be achieved by a moderately suppressed coupling of the scalar with bottom quarks (in comparison with its other Yukawa couplings) and meanwhile a significant enhancement of its coupling with photons (the chargino-mediated loops are capable of doing such a thing under certain conditions). Correspondingly, the couplings of the SM-like Higgs boson deviates from their SM predictions at a level of 10%. If the excesses are corroborated in future, these predictions will serve as the criteria to testify the theory by the precise determination of the scalars' property at next generation e^+e^- colliders [17]. Our results also indicate that the solutions are distributed in three isolated parameter regions with different features. These regions can be further classified into five cases according to their underlying DM physics and the LHC signal, which are summarized in Table 5. The first case in the table is least constrained by current measurements in DM physics and the sparticle search at the LHC, while the second case has been tightly limited by the XENON-1T experiment. All the cases can survive the LHC constraints by the compressed mass spectrum of the Higgsinos with the sneutrino DM, heavy Higgsinos, or the suppression of

$Br(\tilde{\chi}_{2,3}^0 \rightarrow Z\tilde{\chi}_1^0)$. We remind that part of the regions will be explored by updated DM DD experiments and the SUSY search at the LHC, and once new exotic signals are discovered, they will provide complementary information about the EWSB. We also remind that the strong constraints of the XENON-1T experiment on the second case may be avoided in the NMSSM with the inverse seesaw mechanism [42]. The DM physics of this extension is somewhat similar to that of the Type-I extension except that it corresponds to a much more complicated sneutrino sector with several additional parameters, and thus predicts more flexible DM physics.

Acknowledgements

This work was supported by the National Natural Science Foundation of China (NNSFC) under Grant Nos. 11575053.

References

- [1] ATLAS COLLABORATION collaboration, G. Aad et al., *Phys. Lett. B* **716** (2012) 1.
- [2] CMS COLLABORATION collaboration, S. Chatrchyan et al., *Phys. Lett. B* **716** (2012) 30.
- [3] The ATLAS collaboration [ATLAS Collaboration], ATLAS-CONF-2019-005.
- [4] LEP WORKING GROUP FOR HIGGS BOSON SEARCHES, ALEPH, DELPHI, L3, OPAL collaboration, R. Barate et al., *Phys. Lett. B* **565** (2003) 61 [[hep-ex/0306033](#)].
- [5] ALEPH, DELPHI, L3, OPAL, LEP WORKING GROUP FOR HIGGS BOSON SEARCHES collaboration, S. Schael et al., *Eur. Phys. J. C* **47** (2006) 547 [[hep-ex/0602042](#)].
- [6] CMS collaboration, A. M. Sirunyan et al., *Phys. Lett. B* **793** (2019) 320 [[1811.08459](#)].
- [7] CMS COLLABORATION collaboration, Tech. Rep. CMS-PAS-HIG-14-037, CERN, Geneva, 2015.
- [8] ATLAS collaboration, T. A. collaboration, ATLAS-CONF-2018-025.
- [9] S. Heinemeyer and T. Stefaniak, *PoS CHARGED2018* (2019) 016 [[1812.05864](#)].
- [10] J. Cao, X. Guo, Y. He, P. Wu and Y. Zhang, *Phys. Rev. D* **95** (2017) 116001 [[1612.08522](#)].
- [11] F. Richard, [[1712.06410](#)].
- [12] D. Sachdeva and S. Sadhukhan, [[1908.01668](#)].
- [13] P. J. Fox and N. Weiner, *JHEP* **08**(2018) 025 [[1710.07649](#)].
- [14] P. Mondal, S. Maharana and A. Kundu, [[1907.12808](#)].
- [15] U. Haisch and A. Malinauskas, *JHEP* **03** (2018) 135 [[1712.06599](#)].
- [16] T. Biekotter, M. Chakraborti and S. Heinemeyer, [[1905.03280](#)].
- [17] T. Biekotter, M. Chakraborti and S. Heinemeyer, [[1903.11661](#)].
- [18] W. G. Hollik, S. Liebler, G. Moortgat-Pick, S. Paßehr and G. Weiglein, *Eur. Phys. J. C* **79** (2019) 75 [[1809.07371](#)].
- [19] F. Domingo, S. Heinemeyer, S. Paßehr and G. Weiglein, *Eur. Phys. J. C* **78** (2018) 942 [[1807.06322](#)].

- [20] C. Beskidt, W. de Boer and D. I. Kazakov, *Phys. Lett.* **B782** (2018) 69 [[1712.02531](#)].
- [21] K. Choi, S. H. Im, K. S. Jeong and C. B. Park, [[1906.03389](#)].
- [22] T. Biekotter, S. Heinemeyer and C. Munoz, *Eur. Phys. J.* **C78** (2018) 504 [[1712.07475](#)].
- [23] T. Biekotter, S. Heinemeyer and C. Munoz, [[1906.06173](#)].
- [24] U. Ellwanger, C. Hugonie and A. M. Teixeira, *Phys. Rept.* **496** (2010) 1 [[0910.1785](#)].
- [25] U. Ellwanger and A. M. Teixeira, *JHEP* **1410**, 113 (2014) [[1406.7221](#)].
- [26] J. S. Kim, D. Schmeier and J. Tattersall, *Phys. Rev. D* **93**, no. 5, 055018 (2016) [[1510.04871](#)].
- [27] J. Cao, Y. He, L. Shang, W. Su and Y. Zhang, *JHEP* **1608**, 037 (2016) [[1606.04416](#)].
- [28] U. Ellwanger and C. Hugonie, *Eur. Phys. J. C* **78**, no. 9, 735 (2018) [[1806.09478](#)].
- [29] U. Ellwanger, *JHEP* **1203**, 044 (2012) [[1112.3548](#)].
- [30] J. J. Cao, Z. X. Heng, J. M. Yang, Y. M. Zhang and J. Y. Zhu, *JHEP* **1203**, 086 (2012) [[1202.5821](#)].
- [31] M. Badziak, M. Olechowski and S. Pokorski, *JHEP* **1306**, 043 (2013) [[1304.5437](#)].
- [32] J. Cao, F. Ding, C. Han, J. M. Yang and J. Zhu, *JHEP* **1311**, 018 (2013) [[1309.4939](#)].
- [33] K. S. Jeong, Y. Shoji and M. Yamaguchi, *JHEP* **1411**, 148 (2014) [[1407.0955](#)].
- [34] J. Cao, Y. He, L. Shang, Y. Zhang and P. Zhu, *Phys. Rev.* **D99** (2019) 075020 [[1810.09143](#)].
- [35] J. Cao, L. Shang, P. Wu, J. M. Yang and Y. Zhang, *JHEP* **1510**, 030 (2015) [[1506.06471](#)].
- [36] PLANCK collaboration, N. Aghanim et al., [[1807.06209](#)].
- [37] J. Cao, L. Shang, P. Wu, J. M. Yang and Y. Zhang, *Phys. Rev. D* **91**, no. 5, 055005 (2015) [[arXiv:1410.3239](#) [hep-ph]].
- [38] XENON collaboration, E. Aprile et al., *Phys. Rev. Lett.* **121** (2018) 111302 [[1805.12562](#)].
- [39] E. Aprile *et al.* [XENON Collaboration], *Phys. Rev. Lett.* **122**, no. 14, 141301 (2019) [[1902.03234](#)].
- [40] J. Cao, Y. He, L. Shang, W. Su, P. Wu and Y. Zhang, *JHEP* **1610**, 136 (2016) [[1609.00204](#)].
- [41] M. Badziak, M. Olechowski and P. Szczerbiak, *JHEP* **03**(2016) 179 [[1512.02472](#)].
- [42] J. Cao, X. Guo, Y. He, L. Shang and Y. Yue, *JHEP* **10**(2017) 044 [[1707.09626](#)].
- [43] J. Cao, J. Li, Y. Pan, L. Shang, Y. Yue and D. Zhang, *Phys. Rev.* **D99** (2019) 115033 [[1807.03762](#)].
- [44] J. Cao, Y. He, L. Meng, Y. Pan, Y. Yue and P. Zhu, [[1903.01124](#)].
- [45] M. J. Baker *et al.*, *JHEP* **1512**, 120 (2015) [[1510.03434](#)].
- [46] K. Griest and D. Seckel, *Phys. Rev. D* **43**, 3191 (1991).
- [47] D. G. Cerdeno, C. Munoz and O. Seto, *Phys. Rev. D* **79**, 023510 (2009) [[0807.3029](#)].
- [48] D. G. Cerdeno and O. Seto, *JCAP* **0908**, 032 (2009) [[0903.4677](#)].
- [49] S. F. King, M. Muhlleitner, R. Nevzorov and K. Walz, *Nucl. Phys. B* **870**, 323 (2013) [[1211.5074](#)].

- [50] E. Bagnaschi *et al.*, *Eur. Phys. J. C* **78**, no. 3, 256 (2018) [[1710.11091](#)].
- [51] LHC Higgs Cross Section Working Group Collaboration, S. Heinemeyer *et al.*, [[1307.1347](#)].
- [52] K. Choi, S. H. Im, K. S. Jeong and M. Yamaguchi, *JHEP* **1302**, 090 (2013) [[1211.0875](#)].
- [53] U. Ellwanger, *Phys. Lett. B* **698** (2011) 293 [[1012.1201](#)].
- [54] J. Cao, Z. Heng, T. Liu and J. M. Yang, *Phys. Lett. B* **703**, 462 (2011) [[1103.0631](#)].
- [55] F. Staub, *Comput. Phys. Commun.* **185**, 1773 (2014) [[1309.7223](#)].
- [56] F. Staub, *Comput. Phys. Commun.* **184**, 1792 (2013) [[1207.0906](#)].
- [57] F. Staub, [[0806.0538](#)].
- [58] W. Porod and F. Staub, *Comput. Phys. Commun.* **183**, 2458 (2012) [[1104.1573](#)].
- [59] W. Porod, F. Staub and A. Vicente, *Eur. Phys. J. C* **74**, no. 8, 2992 (2014) [[1405.1434](#)].
- [60] P. Bechtle, S. Heinemeyer, O. Stal, T. Stefaniak and G. Weiglein, *Eur. Phys. J. C* **75**, no. 9, 421 (2015) [[1507.06706](#)].
- [61] P. Bechtle, S. Heinemeyer, O. Stal, T. Stefaniak and G. Weiglein, *JHEP* **1411**, 039 (2014) [[1403.1582](#)].
- [62] G. Belanger, F. Boudjema, A. Pukhov and A. Semenov, *Comput. Phys. Commun.* **185**, 960 (2014) [[1305.0237](#)].
- [63] D. Barducci, G. Belanger, J. Bernon, F. Boudjema, J. Da Silva, S. Kraml, U. Laa and A. Pukhov, [[1606.03834](#)].
- [64] G. Belanger, F. Boudjema, C. Hugonie, A. Pukhov and A. Semenov, *JCAP* **0509**, 001 (2005) [[hep-ph/0505142](#)].
- [65] F. Feroz, M. P. Hobson and M. Bridges, *Mon. Not. Roy. Astron. Soc.* **398**, 1601 (2009) [[0809.3437](#)].
- [66] F. Feroz, M. P. Hobson, E. Cameron and A. N. Pettitt, [[1306.2144](#)].
- [67] M. Tanabashi *et al.* [Particle Data Group], *Phys. Rev. D* **98**, no. 3, 030001 (2018).
- [68] G. Altarelli and R. Barbieri, *Phys. Lett. B* **253**, 161 (1991).
- [69] G. Altarelli, R. Barbieri and S. Jadach, *Nucl. Phys. B* **369**, 3 (1992) *Erratum: [Nucl. Phys. B* **376**, 444 (1992)].
- [70] G. Altarelli, R. Barbieri and F. Caravaglios, *Phys. Lett. B* **349**, 145 (1995).
- [71] M. E. Peskin and T. Takeuchi, *Phys. Rev. Lett.* **65** (1990) 964–967.
- [72] M. E. Peskin and T. Takeuchi, *Phys. Rev.* **D46** (1992) 381–409.
- [73] J. Cao and J. M. Yang, *JHEP* **0812**, 006 (2008) [[0810.0751](#)].
- [74] J. de Blas, M. Ciuchini, E. Franco, S. Mishima, M. Pierini, L. Reina and L. Silvestrini, *JHEP* **1612**, 135 (2016) [[1608.01509](#)].
- [75] U. Ellwanger, J. F. Gunion and C. Hugonie, *JHEP* **02** (2005) 066 [[hep-ph/0406215](#)].
- [76] U. Ellwanger and C. Hugonie, *Comput. Phys. Commun.* **175** (2006) 290 [[hep-ph/0508022](#)].
- [77] A. Fowlie and M. H. Bardsley, *Eur. Phys. J. Plus* **131**, no. 11, 391 (2016) [[1603.00555](#)].
- [78] S. Chang, R. Edezhath, J. Hutchinson and M. Luty, *Phys. Rev. D* **89**, no. 1, 015011 (2014) [[1307.8120](#)].

- [79] A. Berlin, D. Hooper and S. D. McDermott, *Phys. Rev. D* **89**, no. 11, 115022 (2014) [[1404.0022](#)].
- [80] A. M. Sirunyan *et al.* [CMS Collaboration], *JHEP* **1803**, 166 (2018) [[1709.05406](#)].
- [81] For ATLAS analyses on supersymmetry search at the LHC, see the website:
<https://atlas.web.cern.ch/Atlas/GROUPS/PHYSICS/CombinedSummaryPlots/SUSY/>.
- [82] U. Ellwanger, G. Espitalier-Noel and C. Hugonie, *JHEP* **1109**, 105 (2011) [[1107.2472](#)].
- [83] M. Farina, M. Perelstein and B. Shakya, *JHEP* **1404**, 108 (2014) [[1310.0459](#)].